Journal of Applied Physics

Evolution of the conductive filament with cycling in TaO_x-based resistive switching devices

Cite as: J. Appl. Phys. **128**, 194501 (2020); https://doi.org/10.1063/5.0032494
Submitted: 08 October 2020 . Accepted: 03 November 2020 . Published Online: 18 November 2020

Yuanzhi Ma, Phoebe P. Yeoh, Liting Shen, Jonathan M. Goodwill, James A. Bain, and Marek Skowronski

Journal of Applied Physics ARTICLE scitation.org/journal/jap

Evolution of the conductive filament with cycling in TaO_x-based resistive switching devices

Cite as: J. Appl. Phys. **128**, 194501 (2020); doi: 10.1063/5.0032494
Submitted: 8 October 2020 · Accepted: 3 November 2020 ·
Published Online: 18 November 2020

View Online Export Citation CrossMark

Yuanzhi Ma,[1] Phoebe P. Yeoh,[1] Liting Shen,[2] Jonathan M. Goodwill,[1] James A. Bain,[2] and Marek Skowronski[1,a)]

AFFILIATIONS

[1]Department of Materials Science and Engineering, Carnegie Mellon University, Pittsburgh, Pennsylvania 15213, USA
[2]Department of Electrical and Computer Engineering, Carnegie Mellon University, Pittsburgh, Pennsylvania 15213, USA

[a)]**Author to whom correspondence should be addressed:** mareks@cmu.edu

ABSTRACT

Physical changes occurring in $TiN/TaO_{2.0\pm0.2}/TiN$ resistive random-access memory devices after prolonged cycling have been analyzed by two scanning transmission electron microscopy modalities: high angle annular dark field and x-ray energy dispersive spectroscopy. In just formed devices, filaments had a shape of a 10 nm diameter Ta-enriched column with the O-rich gap next to electrodes, which was positively biased during electroformation. Devices that failed by stuck-in-high resistance state mode exhibited Ta depletion and oxygen interdiffusion at interfaces with both electrodes akin to effects observed in complementary switching devices. Initially narrow Ta-rich filaments broadened into ~50 nm diameter columns showing speckled contrast due to phase separation. In devices that failed by stuck-in-low resistance state mode, we have observed a strong Ta-enriched sub-filament bridging the gap. The amount of oxygen in the TiN anode in the vicinity of the filament has not changed significantly between as-formed and failed devices, thus indicating that oxygen is not lost during switching. All devices at the end of endurance exhibited interdiffusion of O into TiN and Ti and N into TaO_x.

I. INTRODUCTION

Resistive random-access memory (RRAM) is one of the leading candidates for next generation non-volatile memory applications due to its scalability, long retention, high endurance, and low thermal budget in fabrication allowing for stacking.[1–3] Moreover, RRAM was demonstrated to exhibit multibit encoding showing potential for applications in neuromorphic networks and in-memory computing.[4–6] Among the RRAM cells based on different operating principles, valence-change mechanism (VCM) offers the best values of figures of merit and attracts most attention due to materials compatibility with the CMOS process. For applications such as non-volatile memory or neuromorphic computing, it has been suggested that RRAM should have endurance above 10^{12} cycles. However, most RRAM devices have endurance in the 10^6–10^9 range[7–9] providing motivation for the studies of failure mechanisms.

RRAM devices exhibit several different modes of degradation of electrical properties. The most common are (i) gradual decrease of the high resistance state (HRS) resistance typically ending with stuck-in-low resistance state (LRS) error;[7,10,11–14] (ii) increase of LRS resistance eventually merging with that of HRS (stuck-in-HRS);[7,12,13] and (iii) closing of the window between LRS and HRS at an intermediate value.[9,15] All of the above behaviors have been reported in a set of nominally identical devices undergoing identical testing procedures.[13] Moreover, the failure is typically defined as the resistance of one of the states deviating from the initial resistance by certain set value. In many cases, the devices still could switch or their initial resistances could be recovered by application of a higher voltage pulse of an appropriate polarity.[13]

The interpretations of device degradation are mostly extensions of the VCM mechanism that argues for the creation of oxygen vacancies in the functional oxide by field-induced exchange of oxygen with the anode.[16,17] The oxygen is thought to enter the anode during electroformation and the exchange between the two continues during subsequent switching. This can lead to a gradual increase of the total number of vacancies in the filament and decrease of the device resistance. Eventually, the filament becomes too conductive, sometimes referred to as "strong" or "large diameter," to create a gap and RESET the device.[10,12,14,18] Alternatively, the stuck-in-HRS failure is interpreted as due to redistribution of the oxygen vacancies within the oxide and away from the switching

interface.[13,18] It is not clear why the mobile vacancies cannot move back into the gap. Yet another model suggested that as the defects accumulate in the functional layer with cycling, their mobility increases causing degradation.[15]

The models summarized in the preceding paragraph are based on changes of device I–V with cycling rather than direct monitoring of physical changes within the structure. To date, the only elemental analysis of devices switched multiple times and the changes induced by the repeated switching known to the authors is that of Kumar *et al.*[19–21] These authors have reported ring-like features in their devices, which they associated with lateral outdiffusion of oxygen due to the temperature gradient (Soret effect). With prolonged switching, the entire area of the $2 \times 2\,\mu m^2$ device segregated into what authors interpreted as oxygen-rich and oxygen-poor areas.

Reassessment of failure origin is needed, especially as many assertions of the standard VCM model have been questioned. The formation of the filament was proposed to be due to the lateral motion of ions due to the Soret effect[19–24] in addition to the migration caused by the electric field. Also, new evidence associates the changes in local composition with the motion of metal ions in addition to oxygen.[23–25] These findings opened up new interpretations of failure mechanisms.

In this work, we use two scanning transmission electron microscopy (STEM) modalities, high angle annular dark field (HAADF) and x-ray energy dispersive spectroscopy (XEDS), to study the evolution of the conductive filament due to prolonged electrical stressing of TiN/TaO_x/TiN resistive switching devices. HAADF allowed for monitoring the Ta distribution in the device while XEDS was used to assess the ion exchange between functional oxide and TiN electrodes.

II. EXPERIMENTAL PROCEDURES

Devices used in this study had an inverted via structure, with the bottom electrode and the on-chip integrated load resistor patterned and etched out of 40 nm TiN layer deposited on 1 μm thick thermal SiO_2/Si. This was followed by sputtering of 50 nm thick TaO_x and 10 nm of SiO_x. The active area of the device was defined by e-beam lithography and dry-etching to open up a $150 \times 150\,nm^2$ via through the SiO_x. Devices were finished by sputtering a 40 nm thick TiN top electrode patterned by photolithography and lift-off. Full details of the fabrication and the schematics of the device structure are included in Sec. S1 in the supplementary material.

Devices were formed at a constant source voltage of 12 V with a load resistor of 37 kΩ using the procedure outlined by Ma *et al.*[26] The corresponding device voltage was ∼4 V. Following electroformation, devices were exposed to a train of SET and RESET pulses with a constant amplitude of ±2 V and the pulse width of 10 μs separated by 100 μs intervals. The resistance after each pulse was assessed by a read pulse or sweep with the current limited to below 10 μA. Typical pulse sequence and the circuit used in endurance testing are shown in Fig. S2 in the supplementary material.

The samples for STEM were lifted-out using the same focused ion beam-based procedure as described in our previous publication.[24] STEM images were taken by FEI Themis STEM operating at 200 keV. The HAADF-STEM images were collected using a Fischione model M3000 ADF detector at the inner and outer collection angle of 76.7 and 200 mrad, respectively. The XEDS spectrum images were collected using the four-detector "SuperX" energy dispersive x-ray spectrometer system.

III. RESULTS AND DISCUSSION

A. Electrical testing and electron microscopy

A series of devices were electroformed in positive polarity (positive bias applied to the top electrode) and repeatedly switched between LRS and HRS by applying varying number of pulses in order to follow the filament evolution with cycling. Figure 1(a) shows the resistance changes of a device during 10^3 switching cycles consisting of ±2 V source voltage pulses with R_{LOAD} =10 kΩ in series. The device resistance stayed relatively constant with HRS at 80 ± 10 kΩ and the LRS at 15 ± 2 kΩ, giving an ON/OFF ratio of ∼5.

A cross-sectional HAADF image of a device after testing is shown in Fig. 1(b). The conductive filament appears as a bright column with the diameter of about 10 nm (marked by the arrow). The increased intensity of the HAADF signal within the filament is due to accumulation of the Ta ions by the Soret effect.[23,24] The filament in Fig. 3(a) exhibits weaker contrast than the one reported in our previous publications,[24,27] likely due to the larger thickness of

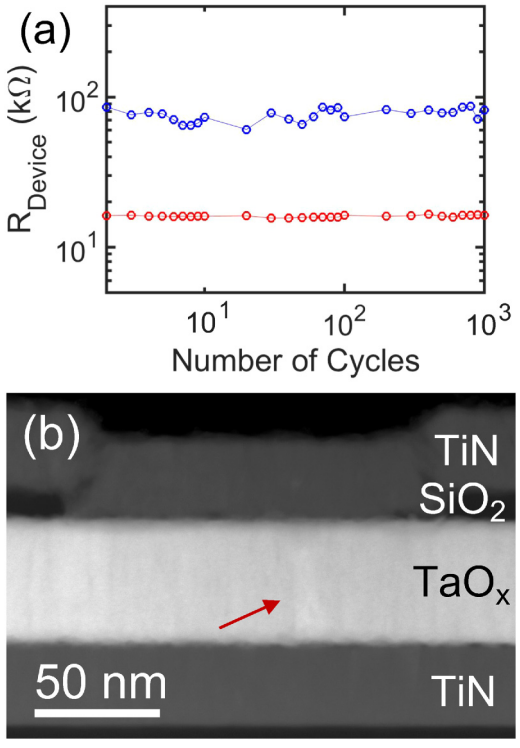

FIG. 1. (a) Plot of device resistance during 10^3 switching cycles. (b) HAADF image of the device in (a) by the end of the 10^3 switching cycles. The testing was stopped with the device in the LRS. The red arrow in (b) marks the location of the filament.

the TEM sample. This reduced the contrast of the filament surrounded by the TaO_x functional layer. One can also notice that the bright column in Fig. 1(b) does not reach the top electrode leaving a ~10 nm wide gap indicating an area with a lower Ta/O ratio and higher resistivity. The location of the gap in the filament is consistent with the direction of the electric field during forming: positive potential of the top electrode caused positively charged Ta ions to move downward. At the same time, negative oxygen ions are expected to accumulate at this interface. One should note that the gap in the filament does not disappear entirely in the LRS. Instead, it is bridged by small diameter sub-filaments typically located at the periphery of filament column. The elemental maps of the device were similar to the ones extensively discussed by Ma *et al.*[27] and are not repeated here.

A total of 41 devices were pulse tested until failure using the same pulse sequence as the one used for Fig. 1. 21 experienced stuck-in-HRS failure and 20 experienced stuck-in-LRS, rendering an almost even chance for device to fail by either one of the failure modes. By failure, here we considered the increase of LRS resistance over 50 kΩ or the decrease of HRS below 10 kΩ. In either case, multiple repeated pulses of the same amplitude failed to change the state of the device. Additional analysis of the electrical switching characteristics is provided in Sec. III B.

An example of the resistivity changes with cycling and two HAADF micrographs of two devices that failed by stuck-in-HRS are shown in Fig. 2. The HRS resistance ranged between 40 and 100 kΩ without exhibiting a clear trend of changes during testing. The LRS resistance gradually increased with stressing and approached the resistance range of HRS failing after 10^5 cycles [Fig. 2(a)].

The HAADF image of the filament in this device is shown in Fig. 2(b) and consists of about 50 nm wide column of speckled contrast. The lateral size of the filament is much wider than the filament in devices that have been just formed or switched for a small number of times [Fig. 1(b) and images in Refs. 24 and 27]. There is no discernible continuous core of the filament, and the gap close to the interface with anode appears to be bridged by one of the speckles. The bright roughly equiaxial speckles are between 5 and 15 nm in diameter with bigger speckles located closer to the center of the column. Similar contrast was reported in the core of some of the filaments.[23,24] Its origin is likely due to phase segregation. The Ta–O system has only two condensed phases (Ta and Ta_2O_5)[28] with the starting composition of the functional $TaO_{2.0}$ film located in the two-phase region. At high temperatures, the uniform $TaO_{2.0}$ is expected to segregate into Ta- and O-rich areas. It is interesting to note that $TaO_{2.0}$ surrounding the bright Ta-rich speckles is slightly darker than the TaO_x layer away from the filament, suggesting local Ta depletion resulting in composition closer to Ta_2O_5.

In addition to the speckled contrast, a dark oval feature with the size of 15 nm is visible in the center of the column. The HAADF intensity in this area is lower than the expected intensity of the Ta_2O_5 inclusion of this size. Since Ta_2O_5 has the lowest volumetric density of Ta ions, this leaves the formation of a void as the only plausible interpretation. Voids forming either within functional layer[29,30] or at functional layer/electrode interfaces[17,31–34] have been reported in RRAM devices numerous times and have

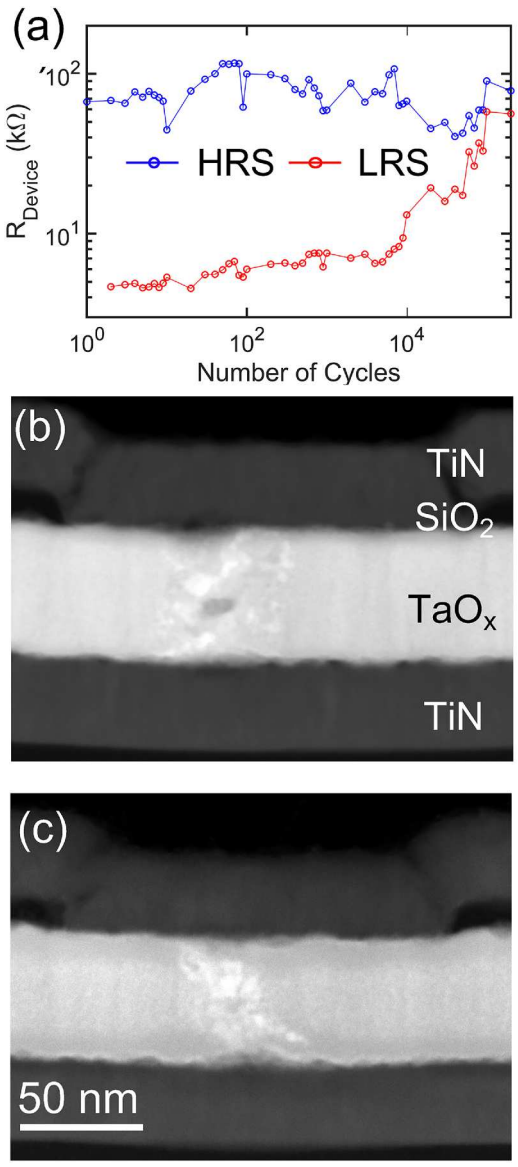

FIG. 2. (a) Resistance as a function of cycling for a device, which failed by stuck-in-HRS. Two examples of the filament shape in HAADF images are shown in (b) and (c).

been typically associated with the evolution of gaseous oxygen,

$$O_O \leftrightarrow \frac{1}{2}O_2(\text{gas}) + V_{\ddot{O}} + 2e'. \quad (1)$$

All of these observations, however, have been reported in devices that have been formed and switched using current compliance of the source-meter or a current source. Neither prevent the discharge of parasitic capacitances in the testing circuit or the

transient current overshoot due to current compliance delays and associated very high temperature excursions.[35,36] Here, such discharges have been greatly reduced by using an integrated on-chip load resistor located next to the device under test.[37] We have never seen voids forming in the device that was just electroformed or switched for a limited number of times. In addition, the location of the void in the middle of oxide layer is not consistent with the reaction (1) which calls for O_2 formation within anode or at its interface with the oxide. The core of the filament is expected to be oxygen deficient. A possible mechanism of void formation is agglomeration of nanopores present in amorphous films deposited at low temperatures. It is widely accepted that such films are not fully dense and contain pores of sizes ranging from a 100 nm to a single vacancy.[38] Upon annealing by the Joule heating due to the repeated switching, the reduction of the surface energy causes voids to agglomerate and form larger voids that are easier to detect. Additional driving force for voiding could be provided by electromigration.[39]

Figure 2(c) shows the HAADF image of another device that failed by the stuck-in-HRS mode. The main characteristics of the filament are consistent with features described above: the filament is wide with diameter of about 30 nm, consists of a speckle contrast, and seems to touch both electrodes at least locally. It also exhibits a dark spot in the center of the layer that could correspond to a nascent void.

The filament morphology in Fig. 2 indicates that with repeated stressing, the filament evolves by converting an increasingly larger volume into Ta-rich and O-rich regions. As the phase segregation progresses, the Ta-rich clusters are expected to grow larger and the number of clusters should decrease. Eventually, the Ta clusters can be completely isolated by the resistive O-rich matrix and make the device's resistance permanently stuck in high resistance state. This failure mode appears to be intrinsic to the thermodynamic properties of sub-stoichiometric TaO_x.

The degree of ion exchange between the TiN electrodes and functional oxide that failed by stuck-in-HRS shown in Fig. 2(b) was assessed by XEDS and is shown in Fig. 3.

Figures 3(b)–3(e) show the XEDS maps while Figs. 3(f)–3(i) contain corresponding line scans. The line scans were obtained from the maps by integration over a 45 nm wide strip marked in the reference HAADF image in Fig. 3(a) as a white rectangle and shown in Fig. S3 in the supplementary material. The red traces represent the line scans at the location of the filament while the black curves were collected away from it and serve as the reference. The horizontal distance scale of each line scan starts at the top of the corresponding XEDS map. The signal-to-noise ratio within the functional layer is too low to interpret changes in the composition within the filament except in the proximity of the electrodes. The signal-to-noise ratio is ~10:1 in areas of high concentration such as O^- in TaO_x or Ti in TiN. Also, the profiles of light elements exhibit a systematic error in form of a non-zero background. The low energy x-ray emissions from the heavier elements produced background interpreted by the XEDS software as emissions from oxygen. Even with these caveats, one can clearly discern the depletion of Ta at both interfaces in Fig. 3(b) as darker areas within TaO_x next to both electrodes. The corresponding red trace in Fig. 3(f) dips below the black line and does not cross it in TiN implying that there is no diffusion of Ta into TiN. Surprisingly,

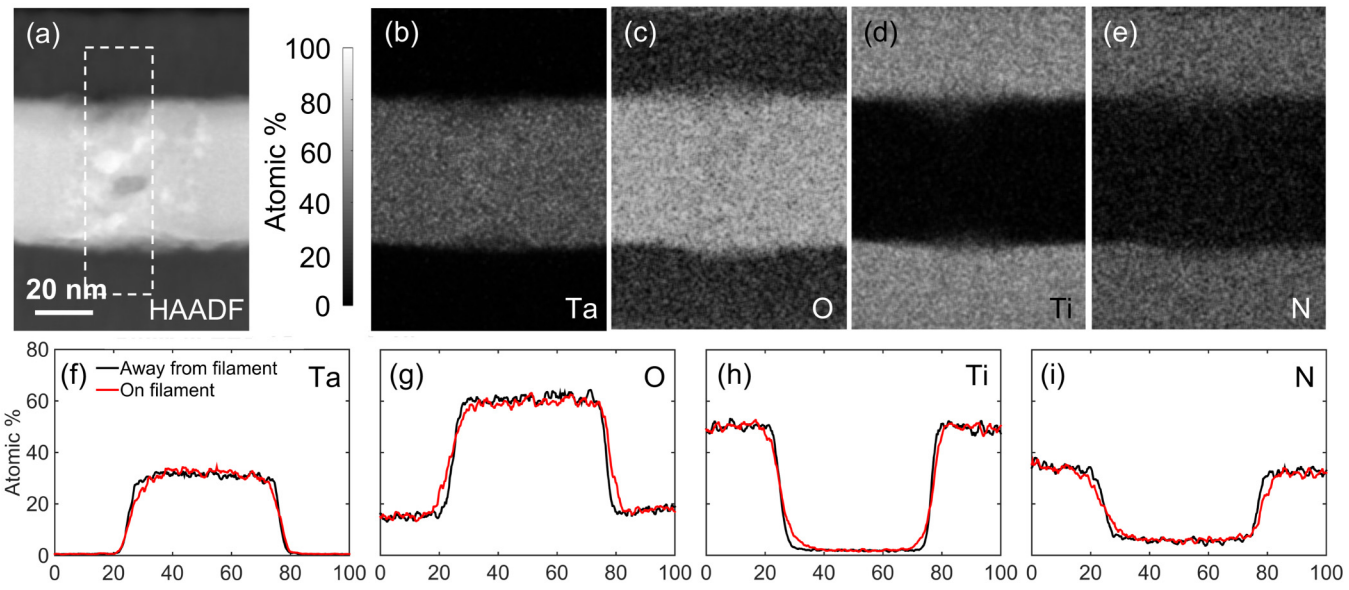

FIG. 3. (a) HAADF image of the device stuck-in-HRS as a reference to elemental maps. Panels (b) through (e) are elemental XEDS maps of Ta, O, Ti, and N of the same area as in (a). Panels (f)–(i) are corresponding line profiles generated by integration of XEDS intensities over the area marked by a white rectangle (red traces). The black traces were integrated over area away from the filament.

this observation applies to both interfaces rather than only the interface with the anode in devices that have been only formed.[27] The map of oxygen distribution [Fig. 3(c)] shows two roughly symmetric domes of increased oxygen content in TiN. This is reflected by the line scan in Fig. 3(g) where the red trace is clearly above the black reference curve in TiN close to either interface: apparently, oxygen diffused into both electrodes in proximity of the filament. Similar observation can be made about Ti and N diffusing into the functional oxide while being depleted on TiN side of the interface. The ion exchange in the device shown in Fig. 2(c) is similar (data included in Fig. S5 in the supplementary material).

The device structures used in this work were symmetric with both electrodes consisting of TiN, yet they exhibit bipolar switching. Inherent asymmetry of bipolar switching is made possible by electroformation, which creates a gap in the filament next to the anode. The gap is bridged in SET processes but is not eliminated during RESET keeping the structure asymmetric. It stands to reason that prolonged switching can reduce or eliminate the initial asymmetry. Such effect was in fact observed in the form of complementary switching.[40–42] The interpretation of this effect relied on the changing position of the gap from one of the electrodes to the other at somewhat higher values of applied voltage and current than during standard switching. Repeated pulsing of the structure can have a similar cumulative effect building a Ta-depleted and O-enriched gap against the other electrode during the SET pulses. This can lead to failure by stuck-in-HRS. The two gaps are opened and bridged in antiphase: when one is opened the other one is bridged. With equally "strong" gaps, one will always be opened with the resistance of the device corresponding to that of HRS. The two types of physical changes in devices (phase separation and formation of two gaps) are independent of each other and either can lead to device failure by stuck-in-HRS.

The observed evolution of devices that failed by stuck-in-LRS mode was different. An example of device resistance as a function of cycling for the device that failed by stuck-in-LRS is shown in Fig. 4(a). The LRS resistance remained stable at about 5 kΩ throughout the entire testing sequence while the HRS randomly changed from 10 kΩ to 80 kΩ before dropping to 5 kΩ after 2×10^5 cycles. The large HRS resistance variability can be explained by the cycle-to-cycle variability of the RRAM cells due to the stochastic nature of the formation of the gap in the filament.[43,44]

Figures 4(b) and 4(c) show the HAADF micrographs of two devices that failed by stuck-in-LRS. Both show a small diameter bright core similar to that of the filament switched only few times [Fig. 1(b)]. In proximity of the top electrode, which served as an anode in electroformation process, the filament strays off to the side with the brighter branch to the left of the core in Fig. 4(b) and right in Fig. 4(c). In Fig. 4(b), a similar but not as pronounced thread-like feature could be seen on the right side as well forming a roughly martini-glass shape. This shape resembles the structure of the filament reported in the device formed to HRS and then switched to the LRS state.[24] In the failed device, however, the sideways shift and contrast due to connecting sub-filament is much stronger akin to the contrast in devices after polarity reversal and the lateral deviation is larger. Apparently, after prolonged cycling, the sub-filament became more Ta-enriched and its diameter became almost as large as that of the filament core.

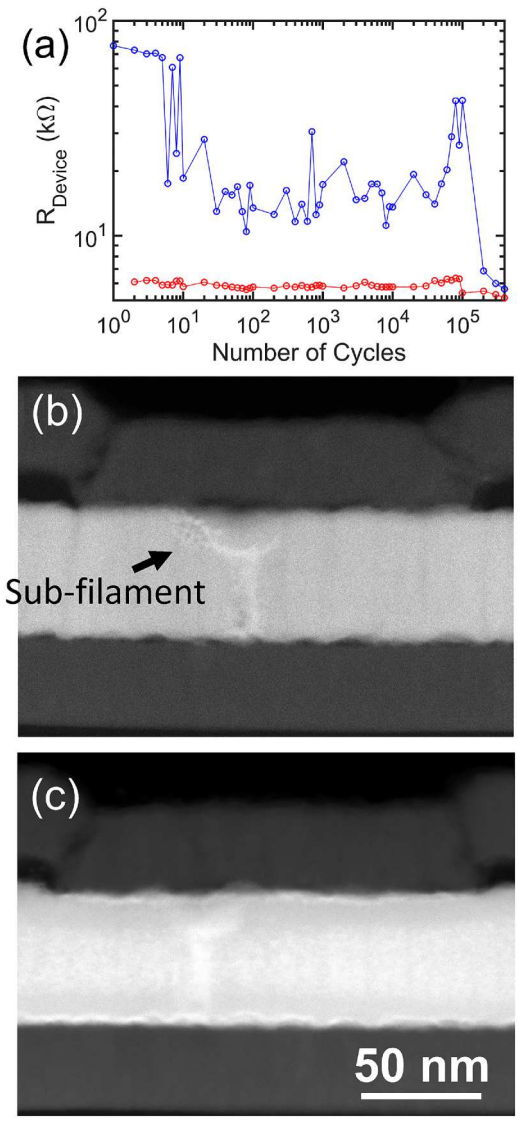

FIG. 4. (a) Resistance as a function of cycling for a device, which failed by stuck-in-LRS. Two examples of the filament shape in HAADF images are shown in (b) and (c).

The reason for the kink in the filament can be gleaned from the micrographs in Fig. 5. Figure 5(a) shows a bright field image of the filament shown in Fig. 4(c). One can easily discern the bright areas corresponding to polycrystalline TiN electrodes on the top and bottom of the image, as well as an hourglass-shape dark feature of the filament. The contrast in bright filed images is due to Rutherford scattering and electron diffraction and is different than contrast in HAADF, which detects electrons scattered by the Rutherford mechanism.

Figure 5(b) shows the high-resolution image of the area at the top of the filament. The image reveals the presence of lattice fringes

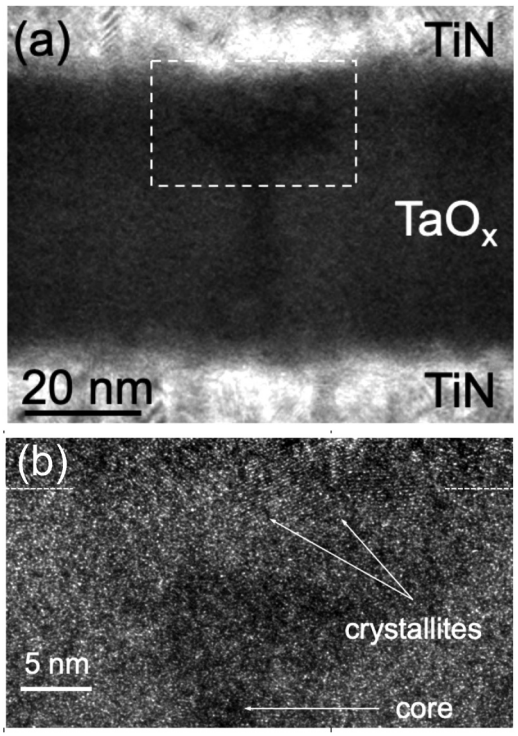

FIG. 5. Bright field image of the filament shown in Fig. 4(c). Panel (b) shows a high-resolution image of the area marked by the dashed box in (a).

within TaO_x at the extension of the filament in the proximity of the top electrode. Gap in the filament is the most likely location for the crystallization of the oxide as it exhibits highest temperatures within the device.[24,27,45] Gap is also the location of the most rapid ion motion connecting or disconnecting the electrodes. The formation of the crystallites impacts this process by reducing the diffusion rates. As a consequence, the conductive sub-filaments bridging the gap in the LRS have to form at the periphery of the polycrystalline region. The temperature distribution follows reaching the maximum at the periphery and causing local crystallization. As the device evolves with cycling, the crystalline region grows and shifts laterally concomitantly with the accumulation of Ta.

The observations described above are in general agreement with the interpretation of the stuck-in-LRS failure mode, which suggested the formation of the strong filament.[12,14,18,46] In most of the publications on the subject, this is assumed to be due to the continued loss of oxygen to the electrode. The elemental distributions mapped out by XEDS and corresponding line scans are shown in Fig. 6. Similarly, as in the case of stuck-in-HRS, one can discern an area of intermixing at the top electrode: depletion of Ta in TaO_x, slight increase of O in TiN, and Ti and N diffusing into TaO_x. In distinction to the HRS, the changes occurred only at the top electrode. The overall depth of the inter-diffused zone and the concentration change is similar but somewhat less than that in the HRS case. The elemental XEDS maps of device in Fig. 4(c) are presented in Fig. S7 in the supplementary material.

A particularly important comparison is that of oxygen distribution right after electroformation and after failure. Figure 7(a) represents the difference between the distribution of oxygen on and off the filament in device that was just electroformed [Fig. 3(g) in

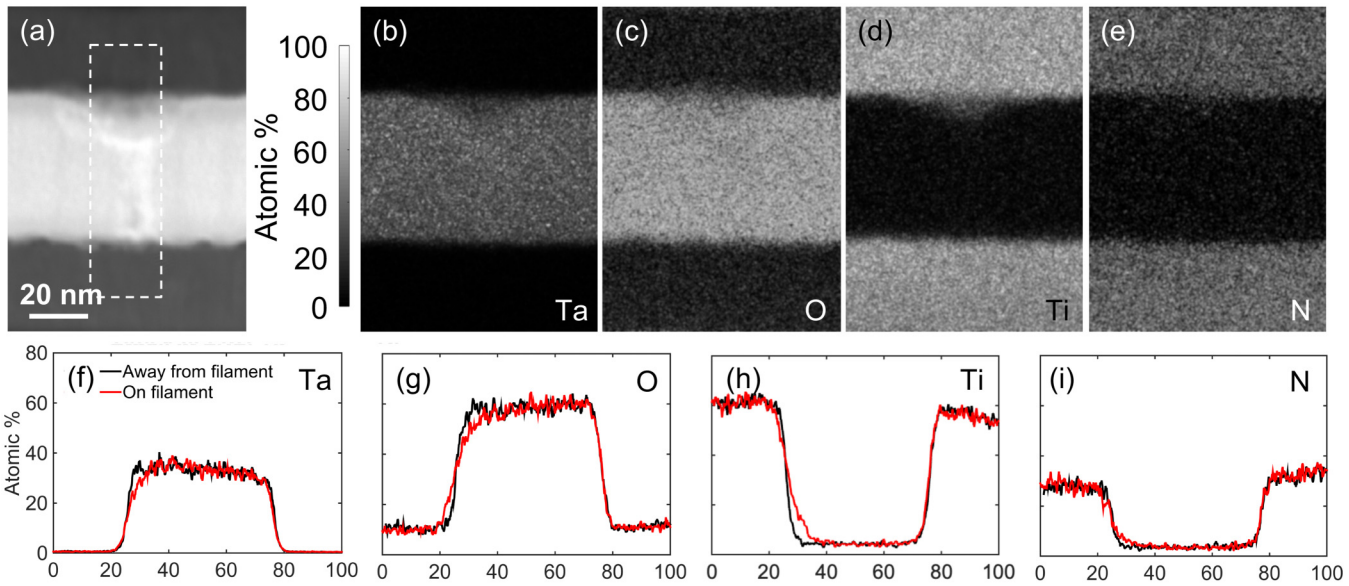

FIG. 6. (a) Reference HAADF images of the filament from Fig. 5(b). (b)–(e) XEDS elemental maps of Ta, O, Ti, and N over the area the same as in (a). (g)–(j) Corresponding line profiles (red traces) were obtained by the integration of the XEDS maps in the area marked in panel (a) by a white rectangle. Black traces were integrated over identical area away from the filament. The distance scale in line profiles starts at the top of each XEDS map.

Ma *et al.*[27]], device stuck-in-HRS [red and black traces in Fig. 3(g)], and device-stuck-in LRS [Fig. 6(g)]. The positions of interfaces between TaO_x and electrodes are marked as black vertical dashed lines. It is quite apparent that the depth of O penetration into TiN and the extent of exchange in all three cases is similar and if anything, the exchange is greater in just electroformed device. One can conclude than that while the interdiffusion does occur during switching as evidenced by the exchange at the bottom interface in panel (b), the total accumulated loss of oxygen during switching is smaller or at most comparable to exchange during formation. The device failure is due to redistribution of oxygen and Ta within the oxide.

At this point it is not clear why nominally identical devices evolve quite differently producing distinctly different filament morphologies. Neither is the role of Ti and N intermixing in evolution of electrical characteristics of TaO_x devices.

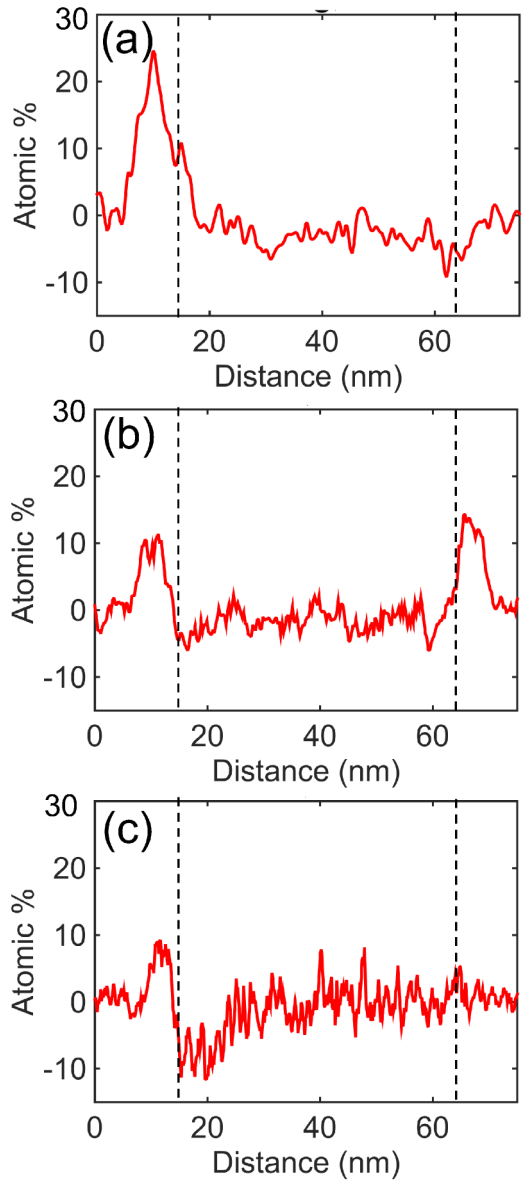

FIG. 7. Difference of oxygen distribution in (a) the device that has been only electroformed (data from Ma *et al.*[27]), device that has failed by stuck-in-HRS, and (c) device that failed by stuck-in-LRS.

B. Endurance vs testing conditions

In order to gain additional insight into the origin of the device failure, we have attempted to differentiate the effect of number of pulses and time-at-bias leading to device failure. We have measured both using pulses with different duration ranging from 1 μs to 1 ms. The results are shown in Fig. 8. For pulses 1, 10, and 100 μs long, the median number-of-pulses before failure stayed almost constant at $\sim 10^5$ cycles decreasing only for the longest 1 ms pulses.

The same data replotted as the total time at bias [Fig. 8(b)] show a decrease of almost two orders of magnitude for shorter pulses. This indicates that it is the temperature transients rather than the time at temperature that are responsible for the failures. Two possible effects could account for the above observation. The first one is a possibility of a capacitive discharge occurring at each switching event. The devices were protected against major current overshoot by the load resistor located on chip right next to the device. This does not, however, eliminate the capacitance of the device itself, the leads, and the resistor serpentine. All of the above will produce a spike of current during switching.[37,47] Moreover, the current flowing through the device is reduced but not entirely eliminated as the capacitance of the cables (~50 pF) still needs to be discharged. The alternative interpretation could be a mechanical fatigue caused by the repeated expansion of the structure.

C. Discussion

The results discussed above are quite different than the ones reported in a series of papers by Kumar *et al.*[19–21] These authors reported oxygen redistribution detected in plan view x-ray absorption maps. With prolonged switching, the entire $2 \times 2\,\mu$m area of devices became rougher and separated into oxygen-rich and oxygen-poor areas with a characteristic lateral size of 100 nm. Increased roughness was interpreted as due to morphology changes of Pt electrode while the lateral oxygen segregation was associated with the Soret effect and nonuniform current flow. This is distinctly different from the results presented here, where changes of oxide composition have been confined to one filament with the diameter below 50 nm. Also, no electrode morphology changes have been observed.

We suggest that these differences originated from the different structures and testing conditions used. Kumar's work has been performed on devices fabricated on thin Si_3N_4 membranes, which together with large power dissipation during electroformation and switching resulted in temperature excursions larger than ones typically experienced by devices fabricated in silicon wafers. This was exacerbated by the lack of an on-chip current limiter, which is known to lead to capacitive discharge resulting in electrode morphology changes.[37] Higher temperatures reached during testing

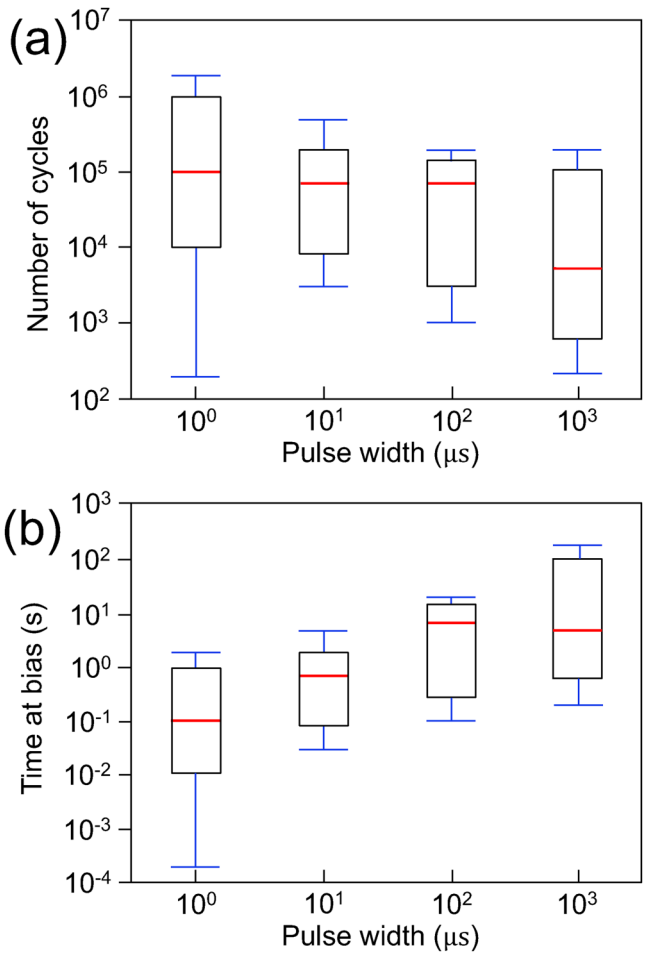

FIG. 8. (a) Distribution of device endurance as a function of pulse length. (b) The same data set plotted as total time at bias vs the pulse length. The red lines correspond to the median; the top and bottom of the black rectangles correspond to the third and first quartiles (Q3 and Q1) of the distribution; the blue bars correspond to the location of 1.5 times of the interquartile range (1.5IQR) above and below the Q3 and Q1, respectively; and the red crosses are outliers that fall outside of the range of [Q1 − 1.5IQR, Q3 + 1.5IQR].

could explain the larger size of segregated areas in the oxide (100 nm in the study by Kumar *et al.* vs 10 nm here) and the appearance of multiple filaments, i.e., multiple electroformation events during testing.

IV. CONCLUSIONS

We have documented the evolution of the filament with prolonged switching and four distinct processes taking place: (i) strengthening of the sub-filament within the gap; (ii) gradual crystallization in the gap area and lateral shift of the filament; (iii) phase separation in the oxide; and (iv) formation of the second gap in symmetric device structures. Three of the above are directly related to device degradation leading to failure by either stuck-in-LRS or stuck-in-HRS modes.

Most of the degradation models to date assumed continued loss of oxygen to electrodes during switching and accumulation of oxygen vacancies in the structure. The above results paint a much more complex picture. While defects do accumulate with cycling, the defects are much more diverse and include Ti and N ions incorporated into the functional oxide. Also, Ta moves not only during electroformation but also during switching, and Ta interstitials should be considered participants in the process. Some oxygen vacancies are created by the exchange with electrodes, but the primary mechanism of creating local nonstoichiometric regions appears to be the redistribution of Ta and O ions within the oxide itself. This, in part, is the consequence of the starting functional oxide, namely, $TaO_{2.0}$, being unstable. Even without temperature or electrostatic potential gradients, this material should segregate into Ta-rich and O-rich regions.

It is quite possible that additional degradation/failure modes exist in devices based on different materials or structures or different testing conditions.

SUPPLEMENTARY MATERIAL

The supplementary material describes details of fabrication and testing of devices used in this study as well as XEDS maps and analysis of two additional devices.

ACKNOWLEDGMENTS

This work was supported in part by the NSF (Grant Nos. DMR-1905648 and SRC 2020-LM-2954). The authors acknowledge the use of the Materials Characterization Facility at Carnegie Mellon University supported by Grant No. MCF-677785. The authors would like to thank Dr. Alexandre Subirats for the discussions related to electrical testing.

DATA AVAILABILITY

The data that support the findings of this study are available from the corresponding author upon reasonable request.

REFERENCES

[1]H. Y. Lee, Y. S. Chen, P. S. Chen, P. Y. Gu, Y. Y. Hsu, S. M. Wang, W. H. Liu, C. H. Tsai, S. S. Sheu, P. C. Chiang, W. P. Lin, C. H. Lin, W. S. Chen, F. Chen, C. H. Lien, and M. J. Tsai, in *IEEE International Electron Devices Meeting* (IEEE, 2010), pp. 19.7.1–19.7.4.
[2]M. J. Lee, C. B. Lee, D. Lee, S. R. Lee, M. Chang, J. H. Hur, Y. B. Kim, C. J. Kim, D. H. Seo, S. Seo, U. I. Chung, I. K. Yoo, and K. Kim, Nat. Mater. **10**, 625 (2011).
[3]T. Liu *et al.*, "A 130.7 mm2 2-layer 32Gb ReRAM memory device in 24nm technology," in *2013 IEEE International Solid-State Circuits Conference Digest of Technical Papers*, (IEEE, San Francisco, CA, 2013), pp. 210–211.
[4]G. W. Burr, R. M. Shelby, A. Sebastian, S. Kim, S. Kim, S. Sidler, K. Virwani, M. Ishii, P. Narayanan, A. Fumarola, L. L. Sanches, I. Boybat, M. Le Gallo, K. Moon, J. Woo, H. Hwang, and Y. Leblebici, Adv. Phys. X **2**, 89 (2017).
[5]M. A. Zidan, J. P. Strachan, and W. D. Lu, Nat. Electron. **1**, 22 (2018).

[6]T. Mikawa, R. Yasuhara, K. Katayama, K. Kouno, T. Ono, and R. Mochida, in *IEEE International Memory Workshop* (IEEE, 2019), Vol. 56.
[7]R. Degraeve, A. Fantini, P. Roussel, L. Goux, A. Costantino, C. Y. Chen, S. Clima, B. Govoreanu, D. Linten, A. Thean, and M. Jurczak, in *Symposium on VLSI Technology* (IEEE, 2015). pp. T188–T189.
[8]Y. Y. Chen, L. Goux, S. Clima, B. Govoreanu, R. Degraeve, G. S. Kar, A. Fantini, G. Groeseneken, D. J. Wouters, and M. Jurczak, IEEE Trans. Electron Devices **60**, 1114 (2013).
[9]M. Azzaz, E. Vianello, B. Sklenard, P. Blaise, A. Roule, C. Sabbione, S. Bernasconi, C. Charpin, C. Cagli, E. Jalaguier, S. Jeannot, S. Denorme, P. Candelier, M. Yu, L. Nistor, C. Fenouillet-Beranger, and L. Perniola, in *IEEE International Memory Workshop* (IEEE, 2016), pp. 1–4.
[10]N. Raghavan, K. L. Pey, D. D. Frey, and M. Bosman, in *Proceedings of IEEE International Reliability Physics Symposium* (IEEE, 2014), p. MY.9.1.
[11]Z. Q. Wang, S. Ambrogio, S. Balatti, S. Sills, A. Calderoni, N. Ramaswamy, and D. Ielmini, in *IEEE International Electron Device Meeting* (IEEE, 2015), p. 7.6.1
[12]C. Y. Chen, L. Goux, A. Fantini, S. Clima, R. Degraeve, A. Redolfi, Y. Y. Chen, G. Groeseneken, and M. Jurczak, Appl. Phys. Lett. **106**, 053501 (2015).
[13]Y. Y. Chen, R. Degraeve, S. Clima, B. Govoreanu, L. Goux, A. Fantini, G. S. Kar, G. Pourtois, G. Groeseneken, D. J. Wouters, and M. Jurczak, in *IEEE International Electron Devices Meeting* (IEEE, 2012), pp. 20.3.1–20.3.4.
[14]B. Chen, J. F. Kang, B. Gao, Y. X. Deng, L. F. Liu, X. Y. Liu, Z. Fang, H. Y. Yu, X. P. Wang, G. Q. Lo, and D. L. Kwong, IEEE Electron Device Lett. **34**, 1292 (2013).
[15]S. Balatti, S. Ambrogio, Z. Wang, S. Sills, A. Calderoni, N. Ramaswamy, and D. Ielmini, IEEE Trans. Electron Devices **62**, 3365 (2015).
[16]R. Waser, R. Dittmann, G. Staikov, and K. Szot, Adv. Mater. **21**, 2632 (2009).
[17]A. Mehonic, M. Buckwell, L. Montesi, M. S. Munde, D. Gao, S. Hudziak, R. J. Chater, S. Fearn, D. McPhail, M. Bosman, A. L. Shluger, and A. J. Kenyon, Adv. Mater. **28**, 7486 (2016).
[18]B. Chen, Y. Lu, B. Gao, Y. H. Fu, F. F. Zhang, P. Huang, Y. S. Chen, L. F. Liu, X. Y. Liu, J. F. Kang, Y. Y. Wang, Z. Fang, H. Y. Yu, X. Li, X. P. Wang, N. Singh, G. Q. Lo, and D. L. Kwong, in *IEEE International Electron Devices Meeting* (IEEE, 2011), Vol. 283.
[19]S. Kumar, C. E. Graves, J. P. Strachan, E. M. Grafals, A. L. D. Kilcoyne, T. Tyliszczak, J. N. Weker, Y. Nishi, and R. S. Williams, Adv. Mater. **28**, 2772 (2016).
[20]S. Kumar, Z. Wang, X. Huang, N. Kumari, N. Davila, J. P. Strachan, D. Vine, A. L. D. Kilcoyne, Y. Nishi, and R. S. Williams, ACS Nano **10**, 11205 (2016).
[21]S. Kumar, Z. Wang, X. Huang, N. Kumari, N. Davila, J. P. Strachan, D. Vine, A. L. D. Kilcoyne, Y. Nishi, and R. S. Williams, Appl. Phys. Lett. **110**, 103503 (2017).
[22]D. B. Strukov, F. Alibart, and R. S. Williams, Appl. Phys. A **107**, 509 (2012).
[23]Y. Ma, D. Li, A. A. Herzing, D. A. Cullen, B. T. Sneed, K. L. More, N. T. Nuhfer, J. A. Bain, and M. Skowronski, ACS Appl. Mater. Interfaces **10**, 23187 (2018).
[24]Y. Ma, J. M. Goodwill, D. Li, D. A. Cullen, J. D. Poplawsky, K. L. More, J. A. Bain, and M. Skowronski, Adv. Electron. Mater. **5** 1800954 (2019).
[25]A. Wedig, M. Luebben, D. Y. Cho, M. Moors, K. Skaja, V. Rana, T. Hasegawa, K. K. Adepalli, B. Yildiz, R. Waser, and I. Valov, Nat. Nanotechnol. **11**, 67 (2016).
[26]Y. Ma, J. Goodwill, and M. Skowronski, in *11th IEEE International Memory Workshop* (IEEE, 2019).
[27]Y. Ma, D. A. Cullen, J. M. Goodwill, Q. Xu, K. L. More, and M. Skowronski, ACS Appl. Mater. Interfaces **12**, 27378 (2020).
[28]S. P. Garg, N. Krishnamurthy, A. Awasthi, and M. Venkatraman, J. Phase Equilib. **17**, 63 (1996).
[29]D. Carta, P. Guttmann, A. Regoutz, A. Khiat, A. Serb, I. Gupta, A. Mehonic, M. Buckwell, S. Hudziak, A. J. Kenyon, and T. Prodromakis, Nanotechnology **27**, 345705 (2016).
[30]G. Martín, M. B. González, F. Campabadal, F. Peiro, A. Cornet, and S. Estradé, Appl. Phys. Express **11**, 014101 (2018).
[31]J. J. Yang, F. Miao, M. D. Pickett, D. A. A. Ohlberg, D. R. Stewart, C. N. Lau, and R. S. Williams, Nanotechnology **20**, 215201 (2009).
[32]D. S. Jeong, H. Schroeder, U. Breuer, and R. Waser, J. Appl. Phys. **104**, 123716 (2008).
[33]D. H. Kwon, K. M. Kim, J. H. Jang, J. M. Jeon, M. H. Lee, G. H. Kim, X. S. Li, G. S. Park, B. Lee, S. Han, M. Kim, and C. S. Hwang, Nat. Nanotechnol. **5**, 148 (2010).
[34]R. Muenstermann, J. J. Yang, J. P. Strachan, G. Medeiros-Ribeiro, R. Dittmann, and R. Waser, Phys. Status Solidi RRL **4**, 16 (2010).
[35]K. Kinoshita, K. Tsunoda, Y. Sato, H. Noshiro, S. Yagaki, M. Aoki, and Y. Sugiyama, Appl. Phys. Lett. **93**, 033506 (2008).
[36]Y. M. Lu, M. Noman, W. Chen, P. A. Salvador, J. A. Bain, and M. Skowronski, J. Phys. D Appl. Phys. **45**, 395101 (2012).
[37]J. Meng, B. Zhao, Q. Xu, J. M. Goodwill, J. A. Bain, and M. Skowronski, J. Appl. Phys. **127**, 235107 (2020).
[38]S. Nakahara, Thin Solid Films **45**, 421 (1977).
[39]Y. C. Chan and D. Yang, Prog. Mater. Sci. **55**, 428 (2010).
[40]S. Balatti, S. Larentis, D. C. Gilmer, and D. Ielmini, Adv. Mater. **25**, 1474 (2013).
[41]F. Nardi, S. Balatti, S. Larentis, D. C. Gilmer, and D. Ielmini, IEEE Trans. Electron Devices **60**, 70 (2013).
[42]S. Kim, S. Choi, and W. Lu, ACS Nano **8**, 2369 (2014).
[43]C. Baeumer, R. Valenta, C. Schmitz, A. Locatelli, T. O. Menteş, S. P. Rogers, A. Sala, N. Raab, S. Nemsak, M. Shim, C. M. Schneider, S. Menzel, R. Waser, and R. Dittmann, ACS Nano **11**, 6921 (2017).
[44]S. Ambrogio, S. Balatti, A. Cubeta, A. Calderoni, N. Ramaswamy, and D. Ielmini, IEEE Trans. Electron Devices **61**, 2912 (2014).
[45]S. Larentis, F. Nardi, S. Balatti, D. C. Gilmer, and D. Ielmini, IEEE Trans. Electron Devices **59**, 2468 (2012).
[46]Z. Wang, S. Ambrogio, S. Balatti, S. Sills, A. Calderoni, N. Ramaswamy, and D. Ielmini, IEEE Trans. Electron Devices **63**, 4279 (2016).
[47]Y. S. Fan, L. Zhang, D. Crotti, T. Witters, M. Jurczak, and B. Govoreanu, IEEE Electron Device Lett. **36**, 1027 (2015).